



EXPERIMENTAL SETUP TESTS FOR A MULTISTAGE PASSIVE CRYOGENIC RADIATOR FOR SPACE APPLICATIONS

Paulo Couto

Marcia B. H. Mantelli

André A. Lopes

Universidade Federal de Santa Catarina

Departamento de Engenharia Mecânica

CP. 476 – Campus Universitário – Trindade

CEP 88040/900 – Florianópolis – SC – Brasil

E-mail: couto@labsolar.ufsc.br

Abstract. *The development of passive cryogenic radiators (PCR) for spacecraft applications is one of the projects of subsystems for satellite thermal control under the frame of a contract between the Satellite Thermal Control Laboratory (NCTS) and the Brazilian Space Agency (AEB). This device is designed to meet the requirements of cooling capacity for infrared radiation sensors and Charged Coupled Devices (CCD cameras) at cryogenic temperature levels. These equipment will be the pay-load of the small-sized Brazilian satellites proposed at the National Program for Space Activities (PNAE). The main objective of this work is to present the experimental setup and data obtained for two prototypes of a small scale multistage PCR. The proposed device is able to meet the need of cooling capacity of 0.1 W @ 150 K at the 1st stage. Double and triple configurations are tested. Experimental data are compared with analytical results and the experimental uncertainties are discussed. The mathematical model developed to predict the temperature distribution and the heat transfer rate in the PCR is briefly discussed.*

Key-words: *Satellite thermal control, Radiator, Cryogenic.*

1. INTRODUCTION

The Satellite Thermal Control Laboratory develops researches on the space field since 1990, when the design of heat pipes and capillary pumped loops begun. Since 1994, NCTS works on the development of spacecraft thermal control subsystems, under several contracts with AEB, which coordinates the PNAE. This program involves Earth Observation Programs, where small scale satellites are proposed for remote sensing missions, telecommunications, meteorology and microgravity experiments. Common payloads on Earth observation satellites are infrared sensors, cloud coverage imaging systems, meteorological radar and CCD cameras. These devices operate at temperature levels below 200 K, presenting a thermal dissipation of 1 W or less (Gilmore, 1995). Cryogenic cooling devices are able to meet these requirements.

Among many known technologies for cryogenic cooling systems, three of them are mostly used: stored-cryogen cooling systems (Gilmore, 1994), active refrigerators (Jewell, 1991) and cryogenic radiators (Donabedian, 1972).

Cryogenic radiators are the simplest way to achieve cryogenic temperatures in space, because the space temperature ($\sim 4K$) is used to absorb the heat dissipated by high emissivity surfaces. Theoretically, radiators can be used to cool down equipments to temperatures about $60 K$ (Wright, 1980), but below $100 K$ the heat rejection capacity falls dramatically due to the T^4 nature of the radiation heat transfer. The main advantage of this technique is the complete passivity of the system, which requires no external power and no moving parts, providing, theoretically, infinite operational life. The main disadvantage is the low cooling capacity ($\leq 1 W$) at low temperatures ($T \leq 100 K$). Even though, Passive Cryogenic Radiator (PCR) are able to attend *PNAE* needs for cryogenic cooling, as shown by Couto & Mantelli (1998).

Figure 1 shows a common configuration for a PCR which is mounted at the *ABRIXAS* satellite (Germany). This device is presented by Brand & Schlitt (1997).

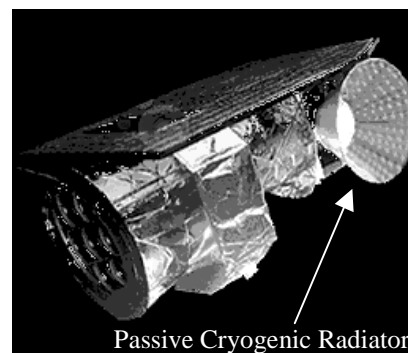


Figure 1 – *ABRIXAS* Satellite (A *B*Road-band Imaging X-ray All-sky Survey Satellite). (Photo courtesy: *OHB Systems – Germany*)

2. PRINCIPLE OF OPERATION OF PCR

The PCR is a satellite thermal control device which takes the wasted thermal energy from a heat source, and discharges it by radiation to the deep space, through high emissivity radiating surfaces, the radiator stages. The PCR stages must be shielded (with a cone, for example) from the direct solar radiation, thermal IR emission and reflected sunlight (albedo) from the Earth. Furthermore, the PCR stages also must be thermally shielded or insulated from the spacecraft structure, to prevent parasitic heat loads. This is usually achieved by the use of Multi-Layer Insulation (*MLI*) and low conductance support systems.

PCR can have one stage (single-stage) or more (multi-stage). The principle of operation of a multi-stage PCR, presented by Wilson & Wright (1977 and 1979) and is showed at Fig. 2, is based on the fact that each stage is thermally isolated from the others by *MLI* and low conductance supports, to minimize the exchange of heat by radiation and by conduction, respectively. Each intermediate stage intercepts the parasitic heat leakage from the insulation below and radiates it to space, allowing the successive radiator stages to have colder and colder temperatures. The lowest temperature is reached at the 1st stage, which is also named *cold plate*.

A prototype of a multi-stage PCR is proposed for ground tests by Couto & Mantelli (1998). The objectives of the tests are:

1. To provide a cooling capacity of $0.1 W @ 150 K$;
2. To validate a mathematical model used to predict the transient temperature behavior;
3. To simulate the space environment on ground tests;
4. To develop the technology on the design and manufacturing of multi-stage PCR.

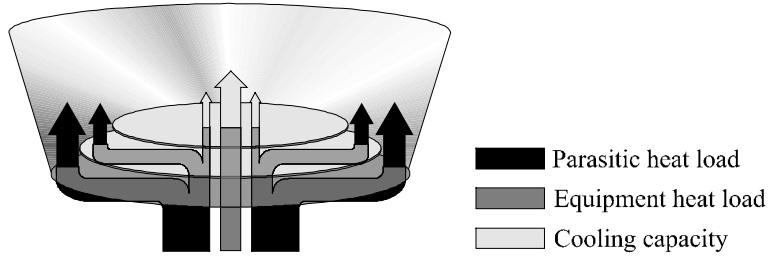


Figure 2 – Principle of operation of multistage PCR.

A multi-stage PCR must have its stage areas optimized in order to reach the lowest possible temperature. Couto & Mantelli (1998) presented a optimization methodology, and the optimized areas are presented in Tab. 1, for single, double and triple stage PCR. Figures 3a and 3b shows the proposed configuration for the triple stage PCR.

Table 1 – Passive cryogenic radiator optimum areas.

	<i>Single-stage PCR</i>	<i>Double-stage PCR</i>	<i>Triple-stage PCR</i>
1 st Stage*	0.02270 m ²	0.01584 m ²	0.01674 m ²
2 nd Stage	-	0.00686 m ²	0.00387 m ²
3 rd Stage	-	-	0.00209 m ²
Total area	0.02270 m ²	0.02270 m ²	0.02270 m ²

*Cold stage

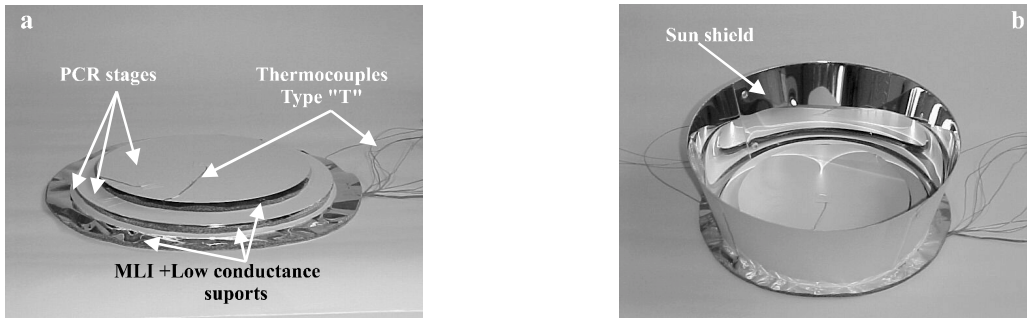


Figure 3 – a) Configuration of the triple stage PCR; b) PCR mounted inside the sun shield.

3. THE MATHEMATICAL MODEL

The mathematical model developed for the prediction of the temperature distribution is fully discussed by Couto & Mantelli (1999) and Couto (1999). This model is proposed to solve the one-dimensional (radial direction), transient, non-homogeneous heat transfer equation, Eq. (1), for each stage and the sun shield, given by:

$$\frac{\partial^2 \Theta_i}{\partial r^2} + \frac{1}{r} \frac{\partial \Theta_i}{\partial r} + \frac{1}{k(T_0 - T_\infty) A_i \delta} q_i = \frac{1}{\alpha} \frac{\partial \Theta_i}{\partial t}, \quad 0 < r < b; \quad t > 0 \quad (1)$$

with the boundary and initial conditions:

$$\frac{\partial \Theta_i}{\partial r} = 0, \text{ in } r = 0; \quad \frac{\partial \Theta_i}{\partial r} = 0, \text{ in } r = b_i; \quad \Theta_i = 0, \text{ in } t = 0 \quad (2)$$

where k is the conductivity of the stage material, α is its thermal diffusivity, A_i is the stage area, δ is its thickness, T_0 is the initial temperature of each stage, T_∞ is the space temperature and Θ_i is the dimensionless temperature of the stage i , given by:

$$\Theta_i(r, t) = \frac{T_i(r, t) - T_\infty}{T_0 - T_\infty} \quad (3)$$

The non-homogeneous term of Eq. (1), say q_i , represents the combination of the heat exchange among the stages, the heat transfer between the stages and the deep space, equipment heat load and environmental heat loads (see Fig.4). The net heat exchange depends on the temperatures of each stage, which is unknown. Therefore, to obtain the temperature distribution, temperatures are assumed to the stages and the heat loads are calculated. Based on these heat loads, the temperature distribution is determined. The average temperature for each stage and sun shield is calculated and the heat generation is obtained. The temperatures are determined again and compared with the input temperatures. This process continues until the convergence is achieved.

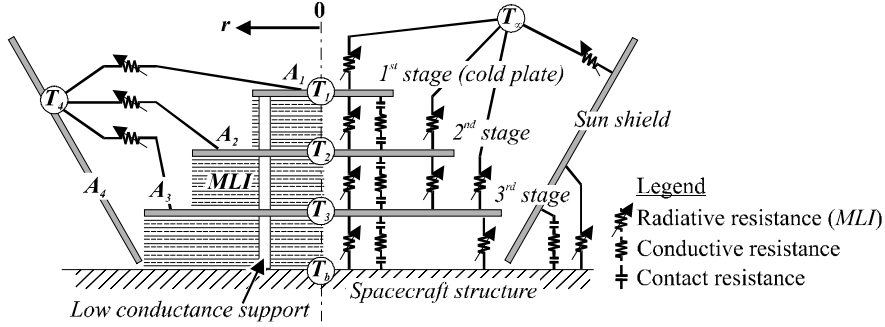


Figure 4 – Thermal resistance network for the triple stage PCR configuration.

The net heat released by each stage is obtained by means of an energy balance over the stage area, as given by:

$$q_i = \left\{ \begin{array}{l} \text{Equipment} \\ \text{heat} \\ \text{load} \end{array} \right\} + \left\{ \begin{array}{l} \text{Parasitic} \\ \text{heat leakage} \\ \text{entering the stage} \end{array} \right\}_{\text{radiative and conductive}} - \left\{ \begin{array}{l} \text{Parasitic} \\ \text{heat leakage} \\ \text{leaving the stage} \end{array} \right\}_{\text{radiative and conductive}} + \left\{ \begin{array}{l} \text{Heat} \\ \text{dissipated} \\ \text{to space} \end{array} \right\} \quad (4)$$

where the *parasitic heat leakage* is the heat loads that passes through the insulation between each successive stage, the *heat dissipated to space* is the cooling capacity of the stage i and the *equipment heat load* is the heat load imposed by the equipment to the stage i .

For the cold plate ($i = 1$), the heat balance given by Eq. (4) is evaluated over the whole stage area (A_1), but for the intermediate stages ($i = 2, 3, \dots$) it is evaluated over two domains of the stage area (A_i): the inner domain, that corresponds to the stage area covered by MLI on both sides, and the outer domain, that corresponds to the stage area covered by MLI on the bottom and exposed to space on the upper side. Figure 4 shows the thermal resistance network used to evaluate q_i on the triple stage configuration. Double and single configurations follow the same network, with the required simplifications. For the double stage configuration PCR, Eq. (4) becomes Eq. (5) for the cold plate, and Eq. (6) and (7) for the inner and outer regions of second stage. For the triple stage configuration, equations for q_i are similar.

$$q_1 = \{Q_{eq,1} + \sigma \varepsilon_{MLI} A_1 (T_2^4 - T_1^4) + U_s (T_2 - T_1) + \alpha [\sigma \varepsilon_4 A_4 F_{41} (T_4^4 - T_1^4)]\} - \{\sigma \varepsilon_R A_1 (T_1^4 - T_\infty^4)\}; \quad (5)$$

$$q_{ext,2} = \{\sigma \varepsilon_{MLI} A_2 (T_b^4 - T_2^4) + \alpha [\sigma \varepsilon_4 A_4 F_{42} (T_4^4 - T_2^4)]\} - \{\sigma \varepsilon_R A_2 (T_2^4 - T_\infty^4)\}; \text{ in } a_2 \leq r \leq b_2 \quad (6)$$

$$q_{in,2} = \{\sigma \varepsilon_{MLI} A_1 (T_b^4 - T_2^4) + U_s (T_b - T_2)\} - \{\sigma \varepsilon_{MLI} A_1 (T_2^4 - T_2^4) + U_s (T_2 - T_2)\}; \text{ in } 0 \leq r < a_2 \quad (7)$$

where $Q_{eq,1}$ is the equipment heat load to be dissipated by the cold plate, ε_{MLI} and ε_R are the MLI and the stages surface emissivities, α is the stages surface absorptivity, T_1 , T_2 and T_4 are

the cold plate, second stage and sun shield temperatures, T_b is the PCR base plate temperature (spacecraft structure), U_s is the global conductance of the low conductance supports and F_{41} and F_{42} is the view factor between the sun shield and the cold plate, and the second stage.

The analytical solution is obtained through the Green Function Solution Equation (*GFSE*) method, as shown by Beck et. al. (1992). The following hypothesis were considered:

- Constant temperature on the PCR base plate (spacecraft structure), $T_b = 300\text{ K}$;
- Space temperature: $T_\infty = 4\text{ K}$ or 77 K to simulate the experimental conditions;
- Each PCR stage and the sun shield are at constant temperature $T_0 = 300\text{ K}$ at $t = 0$;
- The optical and physical properties are temperature invariant.

The solution of Eq. (1) using the *GFSE* with boundary and initial condition (2) is given by:

$$\Theta_i(r, t) = \int_{\tau=0}^t \int_{r'}^i \frac{\alpha}{k} G(r, t, r', \tau) \frac{q_i}{A_i \delta} 2\pi r' dr' d\tau \quad (8)$$

where $G(r, t, r', \tau)$ is the Green Function associated to the solution of the mathematical model, and r' and τ are integration variables. The Green Function $G(r, t, r', \tau)$ can be obtained by solving the homogeneous problem associated with Eq. (1). The solution is:

$$\Theta_i(r, t) = \frac{\alpha}{k} \int_{\tau=0}^t \int_{r'=0}^{b_i} \frac{q_i}{\pi A_i \delta b_i^2} \left[1 + \sum_{n=1}^{\infty} e^{-\beta_n^2 \alpha (t-\tau)/b_i^2} \frac{J_0(\beta_n r/b_i) J_0(\beta_n r'/b_i)}{J_0^2(\beta_n)} \right] 2\pi r' dr' d\tau \quad (9)$$

where the β_n are the eigenvalues, obtained from $J_1(\beta_n) = 0$ and b_i is the external radius of the stage i . Further information are found in Couto & Mantelli (1999) and Couto (1999).

4. THE EXPERIMENTAL SETUP

The experimental setup consists of a liquid nitrogen (LN_2) shroud in a high vacuum environment. Two different PCR prototypes (double and triple configuration) are tested for several levels of heat loads applied to the cold plate by means of skin heaters. The temperatures of the PCR stages and of the sun-shield are monitored.

The LN_2 shroud is shown in Fig. 5a and 5b. It consists of a stainless steel double walled cup, with a volume of 3,1 liter between the stainless steel walls, which is filled with LN_2 . This cup provides temperatures of about 77,4 K (temperature of saturation for the nitrogen) for almost 4,5 hours. The inner surface of the cup is painted with *Solarlack M 40 Li* black paint ($\alpha = 0,95$ and $\varepsilon = 0,86$), to simulate the deep space environment. The outside face of the shroud is covered with adhesive aluminum tape to provide a high reflectance/low emittance surface finishing, aiming its insulation from the incident environmental heat loads (from the laboratory facilities), minimizing the evaporation of the LN_2 inside the shroud. The temperature of the shroud is monitored by four type “T” *AWG40* thermocouples.

The experiment rests over a Teflon base plate, to minimize the heat conduction between the LN_2 shroud and the high vacuum equipment. An electrical heater is bounded to an aluminum base plate (external diameter: 200 mm) and provides enough heat load to keep the base plate at a constant temperature of 300 K. The temperature of the base plate is monitored by three type “T” thermocouples, covering equal measurement areas. Figures 5c and 5d shows the experiment base plate and the skin heater.

A diffusion vacuum pump is used to simulate the high vacuum of space. This vacuum pump is attached to a $3,65 \times 10^{-2} m^3$ volume glass campanula, where the experiments are carried out. This vacuum system is able to keep pressures lower than $1 \times 10^{-6} mbar$.

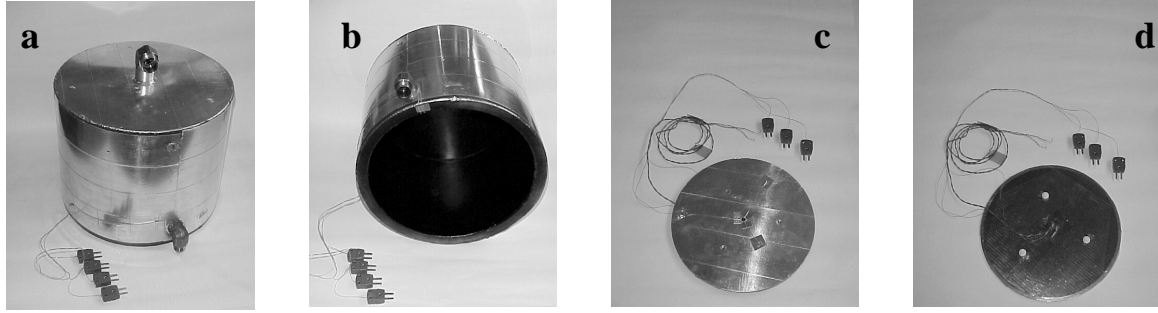


Figure 5 – a) External view of the LN2 shroud; b) Internal testing environment; c) Upper surface of the experiment base plate; d) Skin heater of the base plate.

The PCR prototypes are manufactured at *LABSOLAR/NCTS*, using aluminum sheets made by *ALANOD GmbH & Co.*, Germany. The aluminum is *MIRO C2* quality, with a high reflective surface on one side. The other side is painted with automotive white paint. This paint was chosen due to its low outgassing at high vacuum environment and optical properties (low absorptance and high emissivity). The PCR stages are mounted according Fig 3a and 3b. Low conductance supports and *MLI* are used to provide the insulation between each successive stage. The low conductance supports are made of *Teflon*, and the *MLI* is manufactured with aluminized *Mylar* and *Nylon* net, at the *LABSOLAR/NCTS*. The stage temperatures are measured by three type “T” AWG 40 thermocouples. Heat is supplied at the cold plate and base plate by skin heaters made at LMPT/UFSC. Their electrical resistances are shown in Tab. 2. A *Heinzinger PTN 125-10* power supply unit is attached to each skin heater. The voltage uncertainty of the power supply unit is $\pm 0,005$ V.

Table 2 – Skin heaters resistance.

<i>Configuration</i>	<i>Resistance [omhs]</i>
Triple stage*	$67,741 \pm 0.008$
Double stage*	$68,505 \pm 0.008$
Base plate	$67,550 \pm 0.008$

*Cold stage

An *Hewlett-Packard 34970A* data acquisition unit is used to monitor the temperature of the type “T” AWG40 thermocouples that are installed over the PCR stages and the sun-shield. The resolution of the data acquisition unit is $\pm 0,01 \mu V$. The thermocouples are calibrated at ambient temperature, using a precision *Hg* thermometer, and at $77,4$ K, using liquid nitrogen. At ambient temperature the type “T” thermocouples presented a random error of $\pm 0,1$ K, and at nitrogen saturation temperature, $81,9$ K $\pm 0,2$ K, showing, also, a systematic error of $4,5$ K. This error is considered constant over the measurement range (100 K – 180 K). The uncertainty of the temperature conversion function, given by the manufacturer, is $\pm 0,4$ K. The total random error is ± 0.44 K ($[0,2^2 + 0,4^2]^{1/2}$). So, the measured temperature is given by:

$$T = T_p - 4,5 \pm 0,44 \quad (10)$$

where T_p is the temperature obtained by the conversion equation, given by the thermocouple manufacturer.

The measurement of temperature at cryogenic levels is very difficult to be performed. At such low level of temperature, the heat conduction by the thermocouple wires can affect the measured data. The data acquisition system is at ambient temperature, and to avoid the heat conduction from the data acquisition system, the thermocouple wires are thermally grounded at

the shroud. The heat conduction through the grounded thermocouple wires can be calculated by:

$$Q_{fio} = n \frac{\pi d_w^2 \Delta T}{4L} (k_{Cu} + k_{Co}) \quad (11)$$

where n is the number of thermocouples, d_w is the wire diameter, ΔT is the difference between the average stage temperature and the shroud temperature, L is the wire length and k_{Cu} and k_{Co} are the conductivity of the copper and the constantan wires. For a temperature difference of 60 K between the shroud and the cold plate, the heat transferred through the thermocouple wires is $5 \times 10^{-4}\text{ W}$, while at 150 K the heat irradiated by the cold plate is $0,3\text{ W}$. Therefore, the heat lost by conduction through the thermocouple wires is less than $0,2\%$, being negligible.

Figure 6a shows the experimental mounting. Figure 6b shows the LN_2 shroud and the vacuum system. Figure 6c shows the bell jar with the experimental mounting inside.

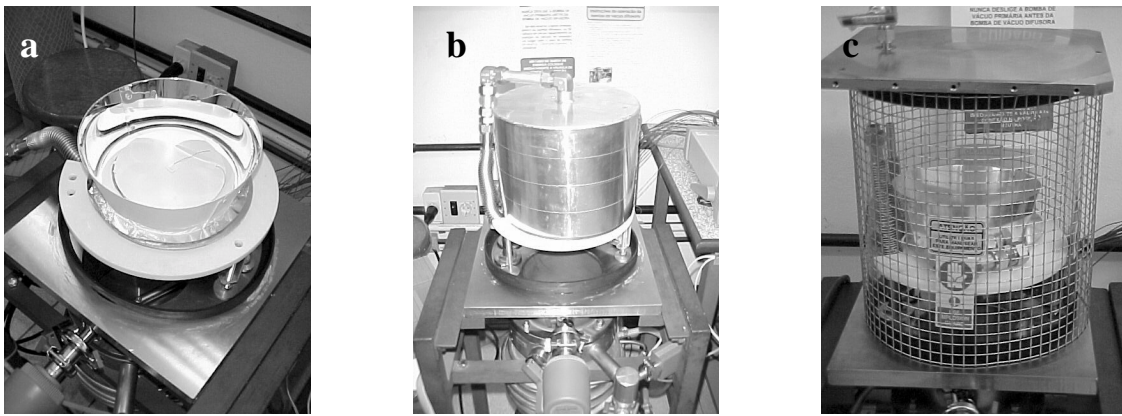


Figure 6 – a) Triple stage PCR mounting; b) LN_2 shroud and vacuum system; c) Experimental mounting inside the bell jar.

5. RESULTS

The test procedure adopted is: 1) evacuation of the vacuum chamber; 2) flood of the LN_2 shroud; 3) experiment temperatures stabilization (with base plate at 300 K), and 4) test setup run. Each test consists of the application of a heat load over the cold plate during two different time periods: $0,61\text{ W}$ during 92 minutes (hot case) and $0,16\text{ W}$ during 35 minutes (cold case). These two levels of heat loads simulates the equipment heat load over the cold plate, say $Q_{eq,1} = 0.1\text{ W}$, plus the environmental heat loads (direct solar energy, Earth IR and albedo) during the sunny part and the eclipse of a hypothetical orbit (equatorial, circular, altitude: 2000 km).

Figure 7 shows the transient temperature as a function of time for the triple stage configuration mounting. Figure 8 shows the experimental data obtained for the double stage PCR configuration. In these figures, experimental data are compared with two extreme theoretical cases of temperature level on the PCR stages. The first theoretical case considers perfect conduction between the low conductance supports and the stages (i.e., negligible contact resistance) as shown by the continuous line in Figs 7 and 8. The second theoretical case considers no conduction on the low conductance supports (i.e., infinite contact resistance) as presented by the dotted line in Figs 7 and 8. The experimental data lays between these two cases, showing that the contact resistance plays an important role on the temperature level distribution. The mean temperature between the two theoretical cases (point-dotted lines in Figs. 7 and 8) is compared with the experimental data. This temperature level corresponds to a contact resistance of about 50 K/W . At a first glance, an experimental contact resistance can be

estimated, by using the experimental temperature data as input data on the mathematical model. The contact resistance obtained appears to be of the same order of magnitude. Accurate data for the contact resistance are still under investigation and will not be presented here.

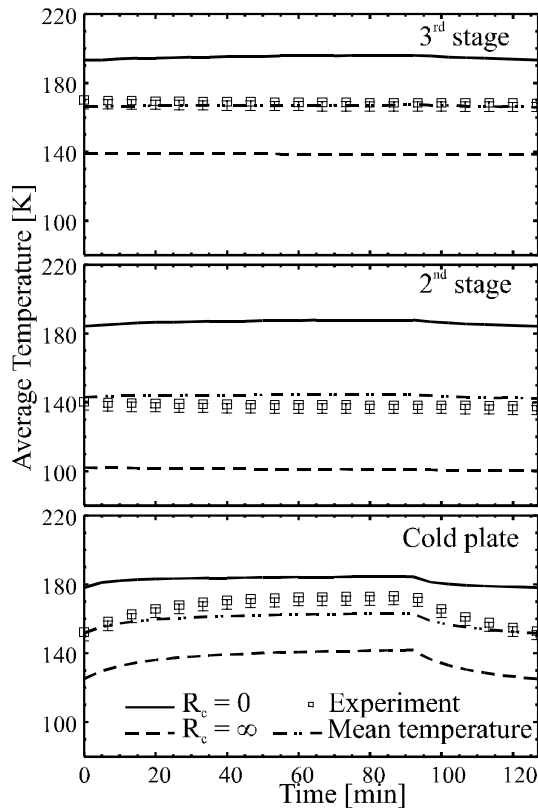


Figure 7 – Transient temperature behavior for the triple stage PCR configuration.

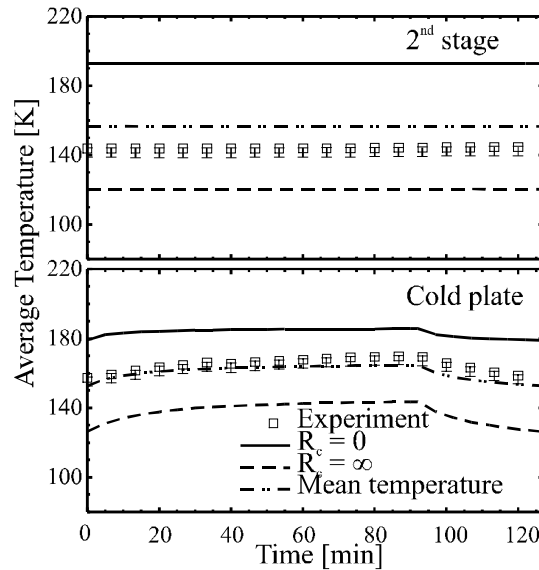


Figure 8 – Transient temperature behavior for the double stage PCR configuration.

Figures 9 and 10 shows the experimental and theoretical steady-state temperatures as a function of the heat load applied to the cold plate. This data was obtained after the cold plate reached the steady state condition. As the applied heat load raises, the difference between the theoretical and experimental data also raises. This occurs because the leakage of part of the equipment heat load, $Q_{eq,1}$, from the cold plate to the second stage was not considered on Eq. (4). This leakage is negligible below a cooling capacity of 0.5 W. As the cooling capacity (or the heat rejection capacity) raises, the temperature of the second stages raises too, raising the cold plate temperature. These figures also show that as the operational temperature raises, the importance of the contact resistances diminishes.

Figure 11 shows the comparison between the experimented prototypes and the existing devices since 1964 (Nimbus I - NASA). The cold plate temperature of the devices is plotted against the ratio between the cold plate area and the equipment heat loads, say A_r/Q_{eq} , for different levels of parasitic heat loads, say Q_p . The closer the device is to the $Q_p = 0$ line, the more efficient it is. Among the presented devices, many had already flown, such as the devices presented by Brand and Schilitt (1997) and Wright (1980). The purpose of the device described in this paper was ground tests. Also, it was manufactured with non-qualified space flight materials. The performance of these devices can be improved by improving the optical and physical properties of the insulation between the stages. This will reduce the parasitic heat load level on the cold plate, and therefore, the temperature of the cold plate. Even though, the PCR developed at LABSOLAR/NCTS presents a better performance of some devices already flown.

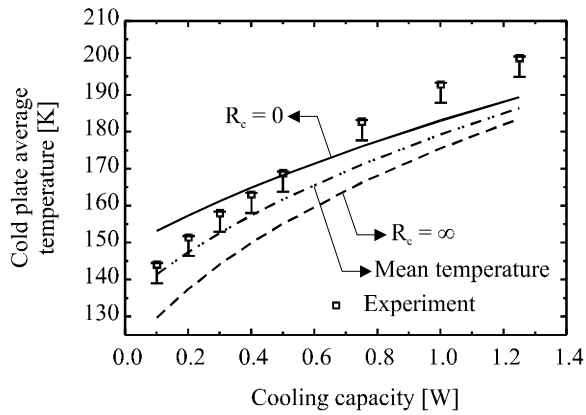


Figure 9 – Cold plate steady-state temperature as a function of the heat load – Triple stage Configuration

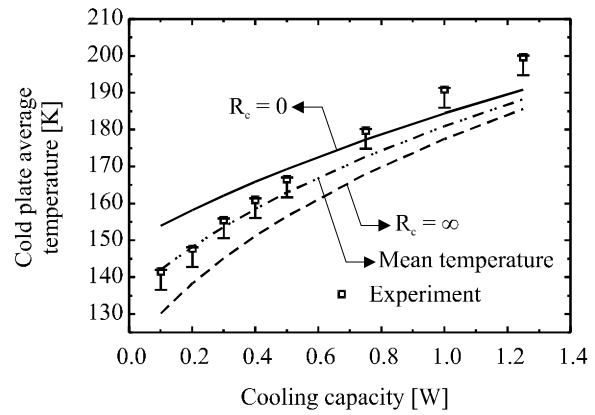


Figure 10 – Cold plate steady-state temperature as a function of the heat load – Double stage Configuration

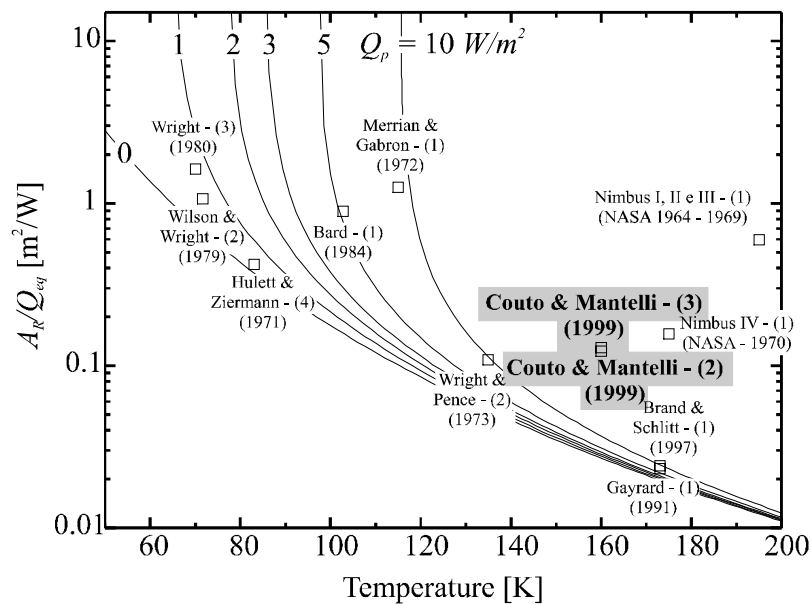


Figure 11 – Comparison between the experimented prototypes and existing devices.

6. CONCLUSIONS

The experimental setup data presented here showed that Multi-Stage PCR is a reliable device for satellite thermal control applications of the Brazilian satellites. The experimental test was performed successfully, and the comparison between theoretical and experimental data is good. The mathematical model hypothesis, discussed in Section 3, showed to be correct. One should note that measurements at very low temperature levels (cryogenic) are very difficult to make. The accuracy of the measurement systems and sensors used at the experiment are compatible with these temperature levels.

The contact resistance between the supports and the stages showed to be a very important parameter on the design of PCR and must be carefully evaluated for future projects.

The results showed that the performance for double and triple stage PCR configurations are similar. Both devices dissipated 0.1 W @ 150 K. The mean bias deviation and the root mean square deviation between the mathematical model and the experiments were -5.8 % and 6.3 % respectively.

The PCR was manufactured at the Mechanical Engineering Department of UFSC, showing that LABSOLAR/NCTS is able to design and develop these cryogenic thermal control device.

Acknowledgments

The authors would like to acknowledge the Brazilian Space Agency – *AEB*, and National Council of Research and Development – *CNPq*, for supporting this project. The authors also would like to acknowledge Dr. Saulo Güths (*LMPT/UFSC*) and Mr. Valtair Garcez (*USICOM/UFSC*) for supporting the manufacturing of the skin heaters and LN_2 shroud, respectively.

7. REFERENCES

- Bard, S., 1984, "Advanced Passive Radiator for Spaceborne Cryogenic Cooling", **Journal of Spacecraft**, Vol. 21, pp. 150–155.
- Beck, J. V., Cole, K. D., Haji-Sheikh, A., and Litkouhi, B., 1992, "Heat Conduction Using Green's Functions", Hemisphere Publishing Co., USA.
- Brand, O. and Schlitt, R., 1997, "Low Temperature Radiator Design for the ABRIXAS X-Ray Satellite", Proceedings of the 6th European Symposium on Space Environmental and Control Systems (ESA SP-400), The Netherlands.
- Couto, P., 1999, "Desenvolvimento e Projeto de Radiadores Criogênicos Passivos para Aplicações Espaciais", M. Sc. Thesis, Mechanical Engineering Department, Federal University of Santa Catarina, Florianópolis, SC, Brazil.
- Couto, P. and Mantelli, M. B. H., 1998, "Sistemas Criogênicos para Aplicações Espaciais", 7th Brazilian Congress of Engineering and Thermal Sciences, Rio de Janeiro – RJ, Brazil.
- Couto, P. and Mantelli, M. B. H., 1999, "A Model to Predict the Transient Temperature Behavior of Multi-stage Cryogenic Radiator", AIAA Paper No. 99-3554.
- Donabedian, M., 1972, "Survey of Cryogenic Cooling Techniques", Aerospace Report TR-0073(3901-01)-1.
- Gayrard, J., 1991, "SIGMA VCHP Radiator: In Orbit Performance", Proceedings of the 4th European Symposium on Space Environmental and Control Systems (ESA SP-324), Italy.
- Gilmore, D. G., 1994, "Satellite Thermal Control Handbook", The Aerospace Corporation Press, El Segundo, CA.
- Hulett, R. H. and Zierman, C. A., 1971, "Staged Radiator Design for Low Temperatures Spacecraft Applications", **Progress in Astronautics and Aeronautics**, Vol. 24, pp. 614-629, Cambridge, MA.
- Jewell, C., 1991, "An Overview of ESA Cryocooler Activities", Proc. of the 4th European Symposium on Space Environmental and Control Systems (ESA SP-324), Italy.
- Merrian, R. and Gabron, F., 1972, "Spaceborne Passive Radiators for Detector Cooling", ASME paper No. 71-Av-30.
- Wilson, D. E. and Wright, J. P., 1977, "The Multistage Heat Pipe Radiator – An Advancement in Passive Cooling Technology", AIAA Paper No. 77-760.
- Wilson, D. E. and Wright, J. P., 1979, "Development and Testing of Two- and Three-Stage Heat Pipe Radiator", AIAA Paper No. 79-1060.
- Wright, J. P., 1980, "Development of a 5 W-70 K Passive Radiator", AIAA Paper No. 80-1512.
- Wright, J. P. and Pence, W. R., 1973, "Development of a Cryogenic Heat Pipe Radiator for a Detector Cooling System", ASME Paper No. 73-ENAs-47.